文章编号：1001－9014(2015)05－0545－06

DOI:10.11972/j.issn.1001－9014.2015.05.006

Terahertz target radar cross-section measurement with ISAR technique

YU Yang, PI Yi-Ming*

(School of Electronic Engineering, University of Electronic Science and Technology of China, Chengdu 611731, China)

Abstract: Researches of RCS include computational electromagnetics and image-based measurement. Restricted by computer memory and operating time, computational electromagnetic methods are difficult to be widely applied in terahertz band. Inverse Synthetic Aperture Radar (ISAR) imaging technique has been commonly utilized in image-based measurement. The reflectivity images are usually reconstructed by back-projection (BP) algorithm. However, the RCS angular glint is significant in terahertz band, which cannot be revealed in the BP images. Thus, the sub-aperture imaging technique was employed to measure the target RCS in terahertz band in this paper. Numerical simulations were adopted to test the validity of the proposed method.

Key words: terahertz, ISAR, RCS, sub-aperture imaging

PACS: 84.40.Xb, 06.30.Ka

基于 ISAR 技术的太赫兹目标 RCS 测量

喻 洋, 皮亦鸣*

(电子科技大学电子工程学院,四川 成都 611731)

摘要:对目标 RCS 的研究主要包括电磁计算与基于成像的测量方法.由于受到计算机内存与运行时间的限制,电磁计算方法难以在太赫兹波段得到广泛应用.在基于图像的测量中常使用逆合成孔径雷达成像技术.后向散射算法(BP)常用于目标的反射图的重建.由于 BP 算法不能在图像中反映太赫兹波段目标显著的角闪烁现象,因此,使用子孔径成像技术对太赫兹目标 RCS 进行测量,并进行了仿真验证所提出算法的有效性.

关 键 词:太赫兹;ISAR;RCS;子孔镜成像

中图分类号:N959.3 **文献标识码**:A

Introduction

The great potential and usefulness of terahertz wave for remote sensing applications have been proved over the past few decades. Although scientists have paid much attention to the terahertz band since at least the 1920s, it still remains one of the untapped frequency bands in the whole electromagnetic spectrum. The biggest challenges in most terahertz applications lie with the target radar cross-section (RCS) of complex targets which can be used for detection, characterization, and radar imagery. Generally, researches of target RCS include computational electromagnetics and image-based measurement methods.

Computational electromagnetics methods can be classified into two categories: numerical methods[1-3] and asymptotic high frequency methods[1,4-5]. Numerical methods are limited by the electrical size of the target measured in wavelength. Thus, as frequency increasing, numerical methods require significant computation time, particularly in terahertz regime. According to the asymptotic methods, the scattered field is calculated as an integral over the complete illuminated surface of the target. However, it is impossible to evaluate this integral for complex targets in terahertz regime.

In the past few years, methods for extracting target RCS from reflectivity images are successively raised. In 1992, approaches that made use of near-field inverse synthetic aperture radar (ISAR) imaging of radar targets and a sophisticated technique using fast cyclical convolution for the image computation were outlined[6]. In 1998, this imaging technique was employed for far-field RCS extraction based on the Fourier transform relation-

Received date: 2014-09-09, **revised date**: 2014-12-02 **收稿日期**:2014-09-09, **修回日期**:2014-12-02

Foundation items:Supported by the National Natural Science Foundation of China (61271287, 61371048, 61301265)

Biography:Yu Yang (1985-), male, [0] Sichuan, Chengdu, Doctorial Student. Research area involves radar target detection in terahertz band. E-mail: carl_yy@163.com

* **Corresponding author**:E-mail: ympi@uestc.edu.cn

ship between the ISAR image and the far-field RCS[7]. In a later paper, this RCS measurement technique was improved further by using the network analyzer calibration in the near-field to far-field transformation[8]. The target reflectivity image was usually reconstructed by applying the back-projection (BP) algorithm[8-12]. Then the direct scattering problem was easily solved by coherently summing the contributions of each point scatterer. However, with the raise of frequency and band-width in terahertz band, imaging resolution increase and the gridding in imaging area substantial expand. As a result, the operation efficiency of BP algorithm greatly decrease in terahertz band. The FFT method was utilized by A. Kayar and M. Katal to reconstruct reflectivity image in X-band, but the imaging result was unsatisfactory[13]. The classical filtered back-projection (FBP) algorithm was also utilized to reconstruct the target reflectivity images[14-15]. However, as BP algorithm, the RCS angular glint cannot be revealed by the imaging method either.

In this letter, ISAR sub-aperture imaging technique is utilized to reconstruct target reflectivity images at different observation angle. Point spread function was used to normalize the RCS curves extracted from each reflectivity images. After that, the RCS in any observation angle can be solved. The method is summarized in Fig. 1.

1 Formulation

1.1 RCS Angular Glint

In optical region, the scattering of an object can be well approximated as a sum of responses from a distribution of independent and non-directional scattering centers. Thus, the target RCS can be expressed as the coherent super-position of each scattering centers as shown below.

$$RCS(\lambda,\theta) = \left| \sum_{i=1}^{N} \sqrt{\sigma_i} \exp[-j4\pi(x_i\cos\theta + y_i\sin\theta)/\lambda] \right|^2 \quad (1)$$

where λ stands for the wave-length of electromagnetic wave, θ denotes the observation angle, σ_i and (x_i, y_i) is the RCS and coordinates of ith scattering center respectively, N is the amount of scattering centers.

In high-resolution radar measurement, each range cell is composed of more than one scattering centers. With the change of observation angle, scattering center position relative to radar also changes, which leads to the fluctuations of RCS in equation . Thus, the echo power of each range cell varies with the observation angle.

In terahertz band, as the wave-length is much smaller than X band, the RCS angular glint is much more significant. For the same scattering center, the echo power varies significantly in different observation angle.

BP algorithm is usually utilized in conventional RCS measurement methods to process 360 degrees target echo data. The reconstructed images show the mean echo power of scattering centers in each range cell. Thus RCS calculation results show great errors due to the influence of angular glint.

1.2 Sub-aperture Imaging Technique

Sub-aperture imaging technique decomposes the full-aperture data to multiple sub-apertures. In each sub-aperture, target rotation angle is considered small enough that echo power of each range cell is fixed. The accuracy of RCS extracted from each sub-aperture images will increase.

The two-dimensional model of target and radar is illustrated in Fig. 2(a). ω stands for the rotation angle speed, (r_i, θ_i) is the instantaneous coordinate of i-th scattering center in polar coordinates system, and ϕ is the observation angle.

The target is irradiated by LFM wave. In practice, in order to decrease the receiver bandwidth, the received signal is usually de-chirped. The de-chirped signal can be presented as

$$s_{if}(\tau,t) = \sum_{i=1}^{N} \sqrt{\sigma_i}\,\mathrm{rect}\left(\frac{\tau - 2R_i/c}{T_r}\right) \cdot \exp[-j4\pi\gamma(\tau - 2R_{ref}/c)R_{i\Delta}(t)/c] \cdot \exp[-j4\pi f_c R_{i\Delta}(t)/c]$$

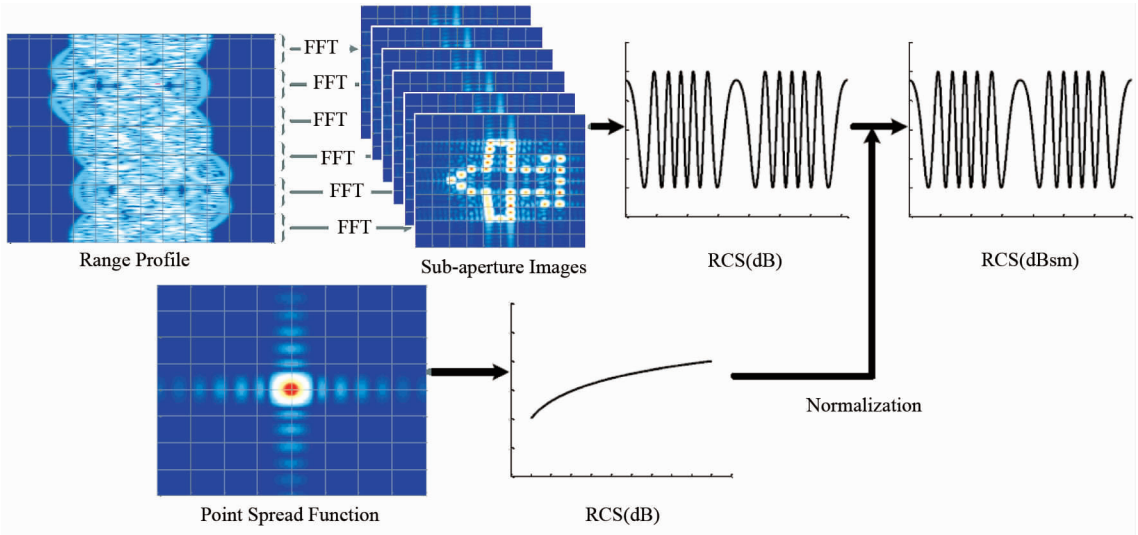

Fig. 1 Summarization of proposed method
图 1 本文所提方法流程

$$\cdot \exp[-j4\pi\gamma R_{i\Delta}^2(t)/c^2] \quad , \quad (2)$$

where c is light speed, f_c is the carrier frequency, γ is the chirp rate, T_r stands for the pulse width, τ and t represent the fast-time and slow-time respectively, rect(τ/T_r) is a square window function, N is the amount of scattering centers, $R_i(t)$ is the instantaneous range between radar and the i-th scattering center which varies with long-time t. $R_{i\Delta}(t) = R_i(t) - R_{ref}$, R_{ref} stands for the reference range.

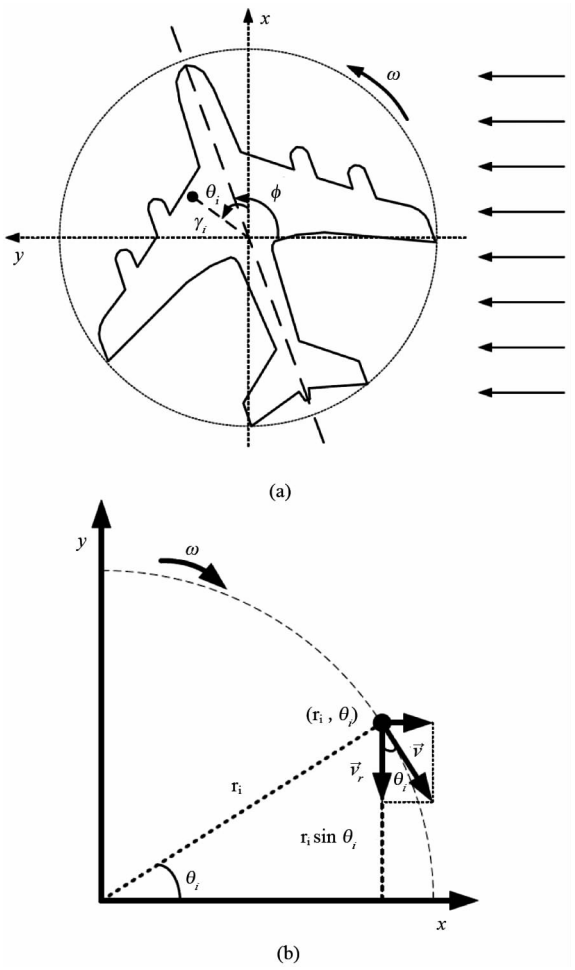

Fig. 2　Geometry of ISAR system. (a) Geometrical parameters of ISAR system; (b) Decomposition of line speed
图 2　ISAR 系统几何关系. (a) ISAR 系统几何参数; (b) 散射点线速度分解

In such case, the spectrum of de-chirped signal can be obtained by Fourier transform of fast-time τ. After carry out the RVP elimination and envelop slant compensation operation, the signal becomes:

$$\tilde{S}_{if}(f_r,t) = \sum_{i=1}^{N} \sqrt{\sigma_i} T_i \,\mathrm{rect}(t/T_a) \cdot \sin[T_r(f_r + 2\gamma R_{i\Delta}(t)/c)] \cdot exp[-j4\pi f_c R_{i\Delta}(t)/c] \quad , \quad (3)$$

T_a stands for the total observation time. Then $\tilde{S}_{if}$ will be divided into sub-aperture signals. Imaging resolution must be considered to determine the width of sub-aperture. Assuming the bandwidth of LFM wave is B, the range and azimuth resolution can be expressed as

$$\rho_r = c/2B \quad , \quad \rho_a = \lambda/2\Delta\theta \quad . \quad (4)$$

To generate image with the same resolution in range and azimuth domain, $\Delta\theta$ should satisfies the equation below:

$$\Delta\theta = \lambda B/c = B/f \quad . \quad (5)$$

So the sub-aperture width is $T_{\mathrm{sub}} = \Delta\theta/\omega$. The signal of m-th sub-aperture can be expressed as

$$G_m(f_r,t) = \sum_{i=1}^{N} \sqrt{\sigma_i} T_r \,\mathrm{rect}\{[t - (m-1)T_{\mathrm{sub}}]/T_{\mathrm{sub}}\} \cdot \sin c[T_r(f_r + 2vR_{i\Delta}(t)/c)] \cdot \exp[-j4\pi f_c R_{i\Delta}(t)/c] \quad , \quad (6)$$

where $m = 1, 2, \cdots, M$, M is the amount of sub-apertures, and the square window function is

$$\mathrm{rect}\left[\frac{t - (m-1)T_{\mathrm{sub}}}{T_{\mathrm{sub}}}\right] = \begin{cases} 1 & \left(m - \frac{3}{2}\right)T_{\mathrm{sub}} \leqslant t \leqslant \left(m - \frac{1}{2}\right)T_{\mathrm{sub}} \\ 0 & \text{otherwise} \end{cases} \quad . \quad (7)$$

In far-field situation, electromagnetic wave can be considered as plane wave. When the rotation center is chosen as the reference point, instantaneous range of i-th scattering center can be approximated as $R_{im}(t) = R_{im} + tv_r(t)$, where R_{im} and (r_i, θ_{im}) stands for the instantaneous range and coordinate of i-th scattering center in m-th sub-aperture when $t = (m-1)T_{sub}$. The angle and range of i-th scattering center in m-th sub-aperture is $\theta_{im} = \theta_{i0} + (m-1)\omega T_{sub}$ and $R_{im} \approx R_{ref} + r_i \sin\theta_{im}$ respectively. Parameter v_r is the radial velocity of i-th scattering center. The line speed of each scattering center can be decomposed as shown in Fig. 2(b). So the radial velocity is $v_r(t) = \omega r_i \cos\theta_i(t)$, Thus, in the m-th sub-aperture, $R_{i\Delta}(t) = r_i \sin\theta_{im} + t\omega r_i \cos\theta_i(t)$. In the sub-aperture interval, observation time is so short that $\cos\theta_i(t) = \cos(\theta_{im} + \omega t) \approx \cos\theta_{im}$. Thus, $R_{i\Delta}(t)$ can be approximated by

$$R_{i\Delta}(t) \approx r_i \sin\theta_{im} + t\omega r_i \cos\theta_{im} \quad . \quad (8)$$

During each sub-aperture interval, the max range migration occurs near the X-axis. If the polar coordinate of scattering center is $(r_i, 0)$, it will turn to $(r_i, \Delta\theta)$ after one sub-aperture interval. The range migration is $\Delta R = r_i \sin\Delta\theta$. Keeping the scattering center stays in the same range cell, ΔR should be less than the range resolution ρ_r. Then we have

$$r_i < c/2B \sin(B/f_c) \quad . \quad (9)$$

Due to the small rotation angle of each sub-aperture, we have $\sin(B/f_c) \approx B/f_c$. Thus the target size should be

$$r_{\max} < cf_c/2B^2 \quad . \quad (10)$$

Under this condition, all the scattering centers stay in the same range cell during the sub-aperture interval, $R_{i\Delta}(t)$ in the sinc function of equation can be replaced by $r_i \sin\theta_{im}$. As a result, the echo spectrum of mth sub-aperture can be represented as below:

$$C_m(f_r,t) = \sum_{i=1}^{N} \sqrt{\sigma_i} T_i \mathrm{sinc}[T_r(f_r + 2\gamma r_i \sin\theta_{im}/c)]$$

$$\cdot \operatorname{rect}\{[t-(m-1)T_{sub}]/T_{sub}\} \cdot \exp[-j4\pi f_c(r_i\sin\theta_{im}+t\omega r_i\cos\theta_{im})/c] \quad (11)$$

The reflectivity image of mth sub-aperture can be reconstructed by Fourier transform of long-time t.

$$\begin{aligned}\psi_m(f_r,f_a) &= \mathrm{FFT}_t[G_m(f_r,t)] \\ &= \sum_{i=1}^{N}\sqrt{\sigma_i}T_rT_a \cdot \operatorname{sinc}[T_r(f_r+2\gamma r_i\sin\theta_{im})/\lambda] \\ &\cdot \operatorname{sinc}[T_a(f_a+2\omega r_i\cos\theta_{im})/\lambda] \\ &\cdot \exp[-j4\pi r_i\sin\theta_{im}/\lambda] \end{aligned} \quad (12)$$

In far-field situation, $r_i\sin\theta_{im}\approx y_{im}$ and $r_i\cos\theta_{im}\approx x_{im}$, where (x_{im},y_{im}) stands for the original Cartesian coordinate of ith scattering center in mth sub- aperture. Substitute f_r and f_a by

$$\begin{aligned} f_r &= -2\gamma y/c \\ f_a &= -2\omega y/\lambda \end{aligned} \quad (13)$$

With (12) and (13), the reflectivity image of mth sub-aperture can be represented as

$$\begin{aligned}\psi_m(x,y) &= \sum_{i=1}^{N}\sqrt{\sigma_i}T_rT_a\operatorname{sinc}[-2\gamma T_r(y-y_{im})/c)] \\ &\cdot \operatorname{sinc}[-2\omega T_a(x-x_{im})/\lambda] \\ &\cdot \exp[-j4\pi y_{im}/\lambda] \end{aligned} \quad (14)$$

Therefore, after 2-dimensinoal Fourier transform, we have the reflectivity image which shows each scattering center on their positions.

1.3 RCS Extraction

The reflectivity image can be represented as a convolution of target impulse response and point spread function (PSF) of imaging system as:

$$\psi(x,y) = h(x,y)\cdot \mathrm{PSF}(x,y) \quad (15)$$

The target impulse response can be expressed as

$$h(x,y) = \sum_{i=1}^{N}\sqrt{\sigma_i}\delta(x-x_i,y-y_i) \quad (16)$$

With equation (1), the target RCS can be represented as

$$\mathrm{RCS}(f,\theta) = \left|\sum_y\sum_x h(x,y)\exp\left[-j\frac{4\pi}{\lambda}(x\cos\theta+y\sin\theta)\right]\right|^2 \quad (17)$$

So the RCS curve extracted from reflectivity image should be normalized by RCS of PSF.

$$\mathrm{RCS}(f,\theta) = \frac{\mathrm{RCS}_\psi(f,\theta)}{\mathrm{RCS}_{\mathrm{PSF}}(f,\theta)} \quad (18)$$

$$\mathrm{RCS}_\psi(f,\theta) = \left|\sum\psi(x,y)\exp[-j4\pi(x\cos\theta+y\sin\theta)/\lambda]\right|^2 \quad (19)$$

For the mth sub-aperture, target rotating angle is $\beta_m=(m-1)\Delta\theta$, the target RCS will be

$$\mathrm{RCS}(f,\phi) = \left|\sum_y\sum_x\sqrt{\sigma_i}\exp[-j4\pi(x_{im}\cos\theta+y_{im}\sin\theta)/\lambda]\right|^2 \quad (20)$$

where

$$\begin{cases} x_{im} = x_{i0}\cos\beta_m + y_{i0}\sin\beta_m \\ y_{im} = y_{i0}\cos\beta_m - x_{i0}\sin\beta_m \end{cases} \quad (21)$$

Assuming $\theta=0$, equation will be

$$\begin{aligned}\mathrm{RCS}_m(f,0) &= \left|\sum_y\sum_x\sqrt{\sigma_i}\exp\left[-\frac{j4\pi}{\lambda}x_{im}\right]\right|^2 \\ &= \left|\sum_y\sum_x\sqrt{\sigma_i}\exp\left[-\frac{j4\pi}{\lambda}(x_{i0}\cos\beta_m+y_{i0}\sin\beta_m)\right]\right|^2 \end{aligned} \quad (22)$$

β_m is the target rotating angle, equals to the observation angle θ in the mth sub-aperture, so we have

$$\mathrm{RCS}_m(f,0)=\mathrm{RCS}(f,\beta_m)=\mathrm{RCS}(f,\theta) \quad (23)$$

Thus the target RCS can be extracted

$$\mathrm{RCS}(f,\theta)=\{\mathrm{RCS}_1 \quad \mathrm{RCS}_2 \quad \cdots \quad \mathrm{RCS}_M\} \quad (24)$$

$$\mathrm{RCS}_m=\mathrm{RCS}_{\psi_m}(f,\theta)/\mathrm{RCS}_{\mathrm{PSF}}(f,0) \quad (25)$$

2 Results

The proposed RCS measuring method has been tested with numerical simulations for a preliminary validation. The carrier frequency is $f_c=0.22$ THz, bandwidth is $B=4.8$ GHz, pulse width is $T_r=1$ ms, PRF is $f_a=100$ Hz, sampling frequency is $f_r=100$ Hz, rotation velocity of turntable is $\omega=1°/s$. The imaging resolution in range domain is

$$\rho_r = c/2B = 0.0313 \text{ m} \quad (26)$$

The rotation angle of each sub-aperture should be

$$\Delta\theta = B/f_c = 0.022 \text{ rad} \quad (27)$$

So the sub-aperture width is $T_{\mathrm{sub}}=\Delta\theta/\omega\approx 1.25$ s, which means that there are 125 pulses in each sub-aperture. Taylor window function is utilized to eliminate the side-lobe in range and azimuth domain. Rotation center is (0,0). The position of scattering centers are (0,-0.001) and (0,0.001). These two scattering centers are reconstructed in the same imaging cell on reflectivity images with different amplitude.

Fig. 3 shows the reflectivity images at different observation angles. Fig. 3(a), (b) are the reflectivity images when observation angle is 0 and 8 degrees respectively. The imaging resolution is greater than the distance of two scattering centers, thus the scattering centers are unresolved in the reflectivity images. This lead to the variation of imaging cell amplitude changes with observation angle, thus the RCS angular glint is well revealed from the sub-aperture images. RCS curve extracted from the sub-aperture images is shown in Fig. 4. It shows the RCS curve extracted by proposed method are consistent with theoretical results, both in shape and values.

To further verify the effectiveness of proposed method, simulation of complicated target is considered. The 10 scattering centers are located at (0,0.001), (0,-0.001), (0.501,0), (0.499,0), (-0.5,0.001), (-0.5,-0.001), (0.001,0.5), (-0.001,0.5), (0,-0.501) and (0,-0.499). The reflectivity images at different observation angle are shown in Fig. 5.

The RCS extracted by proposed method and BP algorithm are shown in Fig. 6. We can see that the RCS curve extracted from sub-aperture images is consistent with theoretical results. In contrast, the deviation of RCS curve extracted from images reconstructed by BP algorithm is much greater due to the influence of target angular glint.

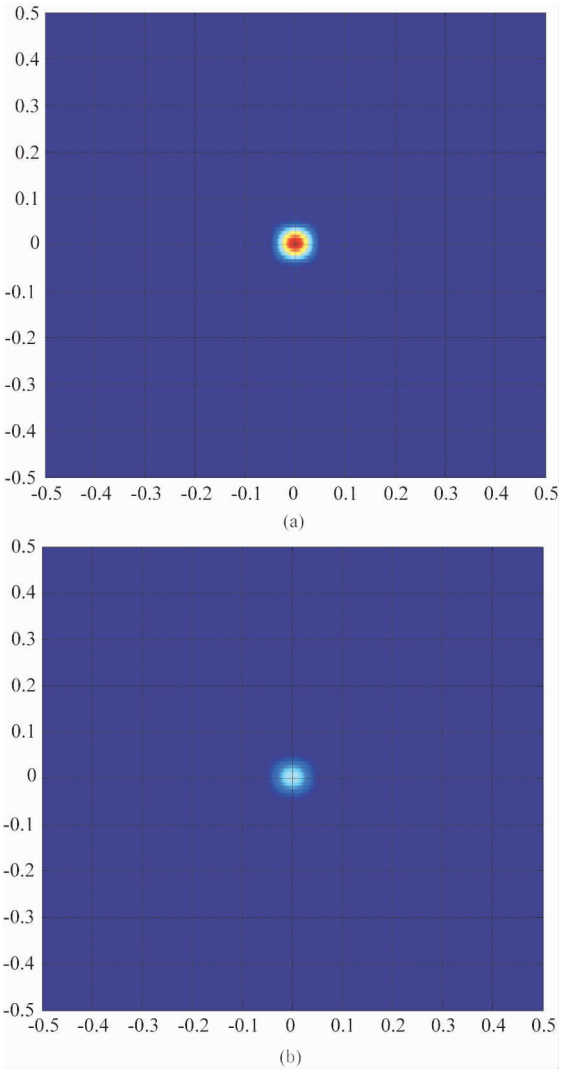

Fig. 3　Reflectivity images at different observation angles: (a) $\theta=0°$; (b) $\theta=8°$

图 3　不同观测角度目标反射幅度图:(a)观测角度为 0°;(b)观测角度为 8°

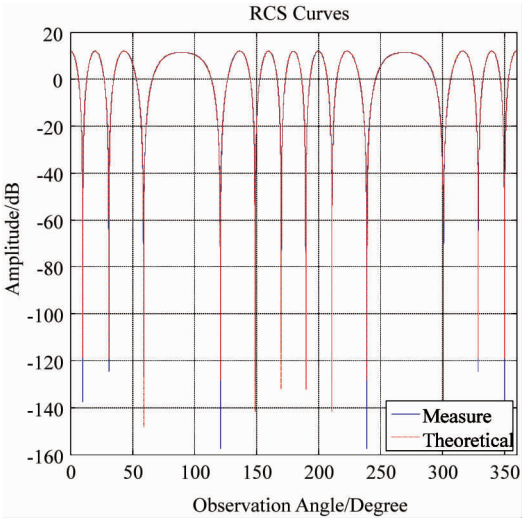

Fig. 4　RCS curves of the target

图 4　目标 RCS 曲线

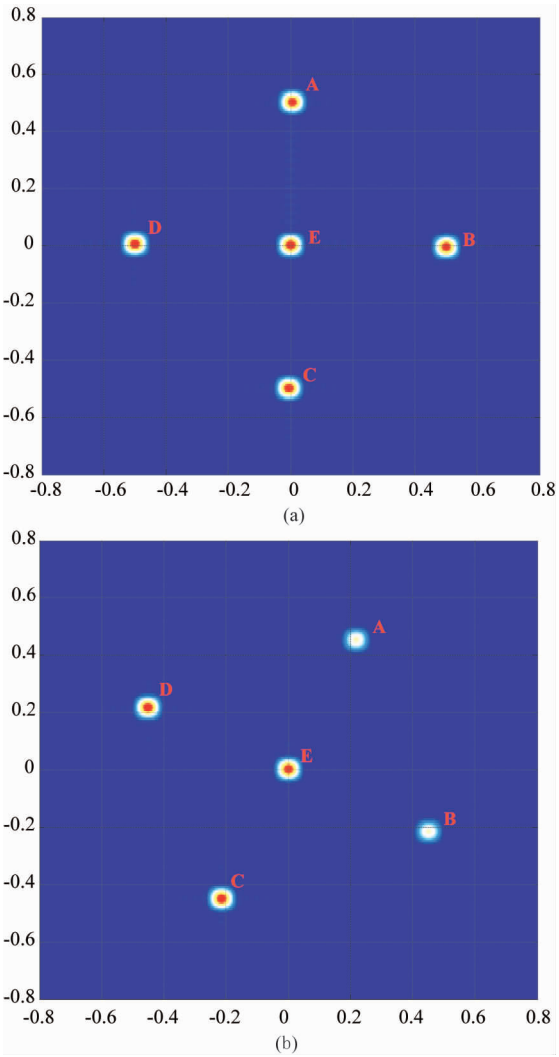

Fig. 5　Reflectivity images at different observation angles: (a) $\theta=0°$; (b) $\theta=25°$

图 5　不同观测角度目标反射幅度图:(a)观测角度为 0°;(b)观测角度为 25°

3　Conclusion

RCS measurement methods are gaining increasing interest in practical problems. In terahertz region, even a small target becomes an electrical large object, which leads to a huge amount of calculation with electromagnetic computing methods. With the raise of frequency, number of scattering centers on target increases, angular glint becomes conspicuous in terahertz band. Thus, traditional RCS measurement methods are no longer applicable in terahertz band.

The RCS measurement methods proposed here utilized sub-aperture imaging technique to reconstruct target reflectivity image at different observation angle. The angular glint and position of scattering centers can be revealed in reconstructed images accurately. Normalized by point spread function, target RCS can be easily extracted from sub-aperture images. Simulations show that the RCS curves extracted by proposed method are consistent with theory both in shape and values.

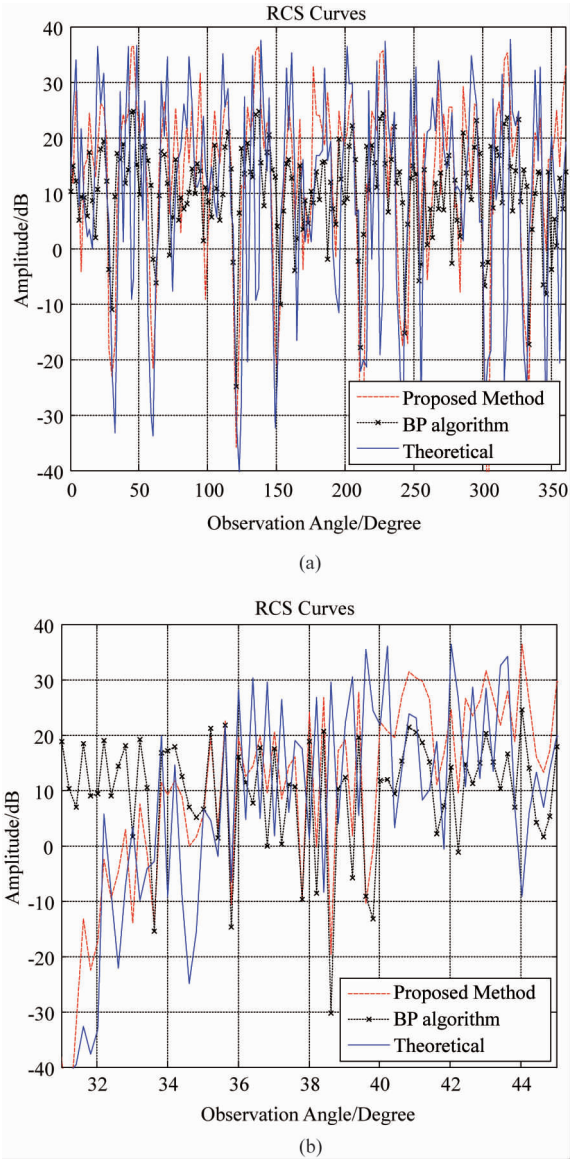

Fig. 6 Target RCS curves: (a) Target RCS curves; (b) Target RCS curves (Details)
图6 目标RCS曲线:(a)目标RCS曲线;(b)目标RCS曲线(细节)

Acknowledgement

This work is supported in part by the National Natural Science Foundation of China under Grant No. 61271287, 61371048 and 61301265. Moreover, we appreciate the reviewers and editors for their careful and patient work, and highly improve the quality of this paper.

References

[1] KNOTT E, SHAEFFER J F, TULEY M T. *Radar Cross Section*[M]. 2nd ed. [S. l.], Boston: Artech House, 1993.
[2] BURKE G, POGGIO A. *Numerical Electromagnetic Code: Method of Moment*[M]. [S. l.], Livermore, CA: Lawrence Livermore Lab., 1981.
[3] SEVGI L. *Complex Electromagnetic Problems and Numerical Simulation Approaches*[M]. [S. l.], Hoboken, NJ: IEEE-Wiley Press, 2003.
[4] XU Feng, JIN Ya-Qiu, Bidirectional analytic ray tracing for fast computation of composite scattering from electric-large target over a randomly rough surface[J]. *IEEE Trans. Antennas Propag.*, 2009, **57**(5), 1495-1505.
[5] BENNANI Y, COMBLET F, KHENCHAF A. RCS of Complex Targets: Original Representation Validated by Measurements—Application to ISAR Imagery[J]. *Geoscience and Remote Sensing, IEEE Transactions on*, 2012, **50**(10), 3882-3891.
[6] BROQUETAS A, JOFRE L, CARDAMA A. A near field spherical wave inverse synthetic aperture radar technique[C]//IEEE. Antennas and Propagation Society International Symposium. Chicago, IL, USA: IEEE, 1992: 1114-1117.
[7] BROQUETAS A, PALAU J, JOFRE L, *et al*. Spherical wave near-field imaging and radar cross-section measurement[J]. *IEEE Trans. Antennas Propag.*, 1998, **46**(5), 730-735.
[8] NICHOLSON K J, WANG C H. Improved Near-Field Radar Cross-Section Measurement Tecnique[J]. *IEEE Antennas and Wireless Propagation Letters*, 2009, **8**:1103-1106.
[9] BURKHOLDER R J, GUPTA I J, JOHNSON J T. Comparison of Monostatic and Bistatic Radar Images[J]. *IEEE Antennas and Propagation Magazine*, 2003, **45**(3), 41-50.
[10] VAUPEL T, EIBERT T F. Comparison and Application of Near-Field ISAR Imaging Techniques for Far-Field Radar Cross Section Determination[J]. *IEEE Trans. Antennas Propag.*, 2006, **54**(1):144-151.
[11] YU Ding, LIU Wei-Long, ZHANG Zhen-Hao. Near field scattering measurement based on ISAR imaging technique[C]//IEEE, Antennas, Propagation & EM Theory (ISAPE), 2012 10th International Symposium on. Xian: IEEE, 2012: 725-728.
[12] GUPTA I J. Computer Code for Imaging, Editing, and Reconstruction of Radar Data: RDIAR[R]. Ohio: The Ohio State University Electro-Science Laboratory, 1995.
[13] KAYA A, KARTAL M. Point Scatterer Model for RCS prediction using ISAR measurements[C]// IEEE. Recent Advances in Space Technologies, 2009. RAST 09. 4th International Conference on. Istanbul: IEEE, 2009: 422-425.
[14] WANG Xiao-Bing, HUANG Xin, WU Ya-Jun, *et al*. Application of Terahertz Technology on RCS Measurement[C]//IEEE. Green Computing and Communications (GreenCom), 2013 IEEE and Internet of Things (iThings/CPSCom), IEEE International Conference on and IEEE Cyber, Physical and Social Computing. Beijing: IEEE, 2013: 1587-1590.
[15] IWASZCZUK K, HEISELBERG H, JEPSEN P U. Terahertz radar cross section measurements[C]//IEEE. Infrared Millimeter and Terahertz Waves (IRMMW-THz), 2010 35th International Conference on. Rome: IEEE, 2010: 1-3.